Plasma Chem Plasma Process (2016) 36:3–28
DOI 10.1007/s11090-015-9660-7

ORIGINAL PAPER

The Role of Transport Phenomena and Modeling in the Development of Thermal Plasma Technology

Maher I. Boulos[1,2]

Received: 15 July 2015 / Accepted: 8 September 2015 / Published online: 4 November 2015

Abstract A brief overview is presented of the principal areas where thermal plasmas had a significant technological impact over the past century. This is followed by an analysis of the specific role played by modelling and studies of transport phenomena under plasma conditions for three specific examples. The first dealing with the development of inductively coupled plasma sources. The following two examples deals with process development for the in-flight melting and spheroidization of powders, and the synthesis of nano-powders. Emphasis is placed on the critical role of plasma–particle interactions under dense loading conditions. A proposal is made for a relatively simple thermodynamic model which can be used for the estimation of the theoretical limits for the processing rates possible with different powders in each of these two cases. The model takes into account radiative energy losses from the surface of the particles and from the formed vapor cloud in the plasma, as well as the residual energy in the gases at the exit of the plasma reactor which are not accessible for process needs.

Keywords Transport phenomena · Heat mass and momentum transfer · Mathematical modeling · Induction plasmas · Plasma-particle interactions · Inflight powder treatment · Nano-powder synthesis

Introduction

Significant advances were achieved over the past four decades in our fundamental understanding of transport phenomena under plasma conditions. These are demonstrated by the development of increasingly more sophisticated two- and three-dimensional

✉ Maher I. Boulos
maher.boulos@tekna.com

[1] University of Sherbrooke, Sherbrooke, QC, Canada

[2] Tekna Plasma Systems Inc., Sherbrooke, QC, Canada

mathematical models backed by solid experimental data for model validation. A brief review is made of major technological advances in the field of thermal plasmas during this period. This is followed by a detailed analysis of the basic phenomena involved, and the role played by modeling in achieving these results. Examples are given of induction plasma source development and its scaling up to the hundreds of kW's power level. The use of induction plasmas for the treatment of powders, and the synthesis of nano-powders is discussed providing basis for process design and experimental validation of process performance.

Overview of Thermal Plasma Technology Development

A schematic representation of the chronology for the development of thermal plasma technology over the past century is given in Fig. 1. Highlight of such developments are presented for different industrial sectors.

Plasma chemical synthesis and metallurgical applications were among the first industrial areas in which thermal plasma technology had its debut [1–3]. The Hüls process was one of the first such processes which went, in the early forties, into full scale industrial production of acetylene from natural gas at the MW power level. The process has evolved with time in terms of both its objectives and the nature of raw material used, which shifted from natural gas to heavy liquid fuels and eventually to coal. The process could not compete, however, in the post-World War II economics, and was eventually abandoned shortly after. Plasma chemical synthesis of pigment grade TiO_2 through the oxidation of $TiCl_4$ in an oxygen plasma flow is another example where plasma process was very competitive and operated on a production scale by Tioxide in the UK.

Numerous large scale applications of thermal plasma technology in the metallurgical industry were also developed in the latter part of the twentieth century [4–10]. These covered such areas as melting and remelting of ferrous and nonferrous alloys, supplementary heating of blast furnaces, scrap melting in a transferred arc or cupola furnaces, aluminum recovery from dross, and tundish heating in the continuous casting process. Tundish heating [11–13] is among the most successful applications which survived the test

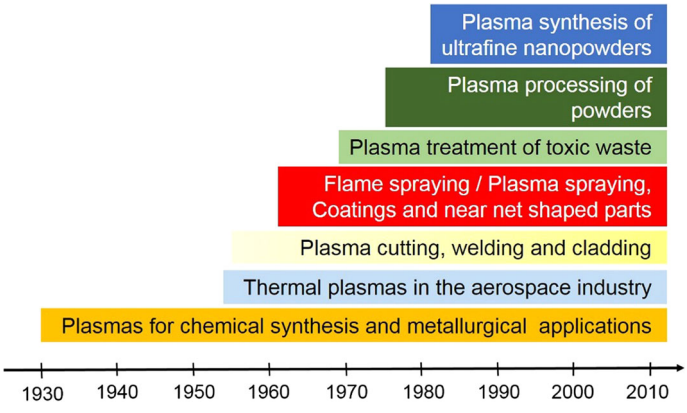

Fig. 1 Chronological evolution of some of the main industrial applications of thermal plasma technology over the past century

of time. In these applications the plasma provided a unique advantage of rapid and controlled localized heating, that could not be matched by alternate lower cost technologies.

Thermal Plasma wind tunnels for the testing of materials under re-entry conditions, is an example of a highly successful application of thermal plasma technology in the aerospace industry [14–16]. In this case, the plasma source provides unique capabilities of simulating the high temperature environment to which materials are exposed during re-entry to the earth atmosphere. The requirement being both in terms of energy level and chemistry of the medium. High power thermal wind tunnels have mostly been built in the sixties and seventies in the USA, Europe and the former Soviet Union using segmented dc plasma torches operating at power levels up to 70 MW. A number of rf induction plasma systems have also been built for operation at reduced pressures and supersonic flow conditions at power levels up to 1 MW [17]. A renewed interest in this type of installations (both DC and RF plasma sources) has emerged over the past few years.

Plasma cutting, welding and Plasma Transferred Arc (PTA) coating have been well established for many decades. The world market for plasma cutting and welding equipment's in 2009 was estimated at around 12.8 Billion US$. The technology lends itself to fully automated robotic control operation with high quality cutting of thick plats which is complementary to water-jet cutting, laser cutting and traditional mechanical cutting [18–20]. Plasma welding represents even a larger field than plasma cutting, which according to Hirata [21] is in the trillion US Dollar range, worldwide. Plasma cutting includes, among others, such technologies as Gas Tungsten Arc Welding (GTAW), Tungsten Inert Arc (TIG), Gas Metal Arc Welding (GMAW) Metal Inert Gas (MIG), and Submerged Arc Welding (SAW). Reviews on the subject can be found in a number of text books [19, 22, 23] as well as numerous papers in scientific journals [24–29]. PTA coating technology is mostly used on an industrial-scale for laying thick coating, for corrosion and wear resistant applications in the mining and petroleum drilling industry [30]. The process is significantly different from the other coating processes as the surface of substrate is locally molten in the process creating a strong metallurgical bond between the coating and the substrate.

Plasma spraying, coatings and deposition of near net shaped parts is an application where thermal plasma technology offered means of extending flame spray technologies to new levels especially for the deposition of refractory metals and high melting temperature ceramics [30–33]. The process is based on the in-flight heating and melting of powders in a plasma jet followed by the deposition of the formed molten droplets onto the surface of the substrate where they form a coating through successive overlaying of splats. In contrast to PTA, the substrate temperature is independently controlled and rarely reaches above a few hundred degrees Celsius. The process can be carried out in an open atmosphere (APS), or under controlled conditions (CAPS), or under vacuum (VPS). The feed materials are mostly in the form of powders, though in certain cases wires, cords, solutions or suspensions are used. The technology was initially introduced in the aerospace industry in the fifties and sixties. Over the past four decades its use expanded significantly to the chemical and mining industry, the electronic industry and more recently in the automotive and biomedical fields. Globally, plasma spraying represents about 50 % of the thermal spray market which was estimated in 2012, to be about 4.6 billion US$.

Plasma treatment of toxic waste has emerged in the in the eighties as a possible potential application of thermal plasma technology. It was initially considered as the optimal solution for the destruction of hazardous or carcinogenic products such as Polychlorinated Biphenyls (PCB's) [34–38]. The technology was also extended to the vitrification of fly ash and of radio-active waste. The treatment of medical and even municipal waste was also considered. Unfortunately, the processing cost is relatively high, which

limited the further development of the technology to niche applications such as the treatment of medical waste and of waste materials on ships, the vitrification of fly ash and radio-active waste, and the destruction of toxic mineral waste. Over the past decade, the concept of waste-to-energy conversion was introduced by the Plasco Group on a commercial production scale in Ottawa, ON, Canada. The process combines the plasma treatment with conventional municipal waste gasification process, with an overall positive energy balance, which contributed favorably to its overall balance sheet.

The plasma processing of powders has emerged as one of the most promising approaches for the purification, densification and spheroidization of powders [30, 39–42]. The process is based on the in-flight heating and melting of the feed material followed by its gradual cooling and solidification in the form of dense spherical powder. The main advantage of induction plasmas was the excellent control of the purity of the material being processed, combined with a flexibility of the plasma chemistry and the overall processing conditions. The process is applicable to ceramic, pure metallic and alloy powders. The feed stock being either in the form of a crushed angular, or agglomerated powder with a diameter that can vary between tens to the hundreds of microns. The main characteristics of the processed powder is their perfectly spherical particle shape, high packing density and generally improved purity and flowability.

The plasma synthesis of nano-powders and nano-structured materials is another example of a rapidly emerging, plasma-based, technology in which the precursor of the material processed is vaporized under plasma conditions, followed by the rapid quench of the formed vapor cloud [43–47]. The process allows for the use of a feed stock in the form of a fine powder, a suspension, a liquid or even a gaseous precursor. Through the control of the chemistry and the processing conditions in the plasma, it is possible to generate a nano-powder with identical chemistry as the feed stock, or with a significantly shifted chemistry with a close control on the morphology and the particle size distribution of the powder obtained. The process has been successfully used for the synthesis of metallic powders such as nano-aluminum, nano-copper, nano-nickel, and nano-silicon for a wide range of applications in the electronic industry. It has also been used for the generation of nano-powders of oxide ceramics such as nano-alumina, nano-zinc oxide, nano-glass, and Boron Nitride Nano Tubes (BNNT). At the moment the process, which is in rapid development, is limited to high added value materials due to its high specific energy requirement. The economics of the process evolves positively with its scale-up to industrial scale, high production levels.

Examples of Plasma Source and Process Technology Developments

Throughout most of the applications reviewed above, fundamental studies of transport phenomena under plasma conditions, coupled with mathematical modelling, and diagnostics, played a key role in the development of the technology on a solid scientific basis. Three examples are given of such developments. The first dealing with the development of the induction plasma source for R&D and industrial scale processing of materials. The following two examples given are dealing with the processing of powders under plasma conditions for their purification, densification, and spheroidization, and the synthesis of nano-powders using induction plasma technology.

Induction Plasma Source Development

The basic concept of induction heating of gases can be traced back to the beginning of the twentieth century when Hewitt introduced in 1904, the concept of the induction lamp. This was followed in 1945 by Babat who introduced the concept of E and H coupling into a plasma, followed by Reed [48] who was the first to operate an rf induction plasma torch in an open flowing discharge mode. A representation of the milestones that followed in the development of the induction plasma torch as we know it today is shown in Fig. 2. These show the segmented metallic wall version proposed by Dresvin and his collaborators at the Technical University of St Petersburg, in the former Soviet Union [49]. This is followed by the TAFA torch developed by M. Thorpe and his collaborators [50] under NASA contracts in the USA, and the segmented torch proposed by Reboux in France in the seventies.

In the eighties and nineties, Yoshida, Akashi and their collaborators [51–53], at the University of Tokyo, proposed the dc–rf hybrid torch which successfully combined the dc and rf torch technologies. This was followed by Jurewicz and Boulos and their collaborators [54–59] at the University of Sherbrooke, QC, Canada who developed the ceramic-wall induction plasma torch which was later licensed to Tekna Plasma Systems Inc. for further development of the technology on an industrial scale.

The basic design of the, patent protected, Tekna ceramic-tube induction plasma torch is shown in Fig. 3. This features the following;

- The use of a high thermal conductivity, thermal shock resistant ceramic tube for the plasma confinement tube.
- The external cooling of the ceramic tube using high velocity, laminar film cooling water.
- The encapsulation of the water-cooled copper induction coil into a polymer-matrix composite which allows for the precision machining of the inner surface of the cooling-water cavity in order in insure precise control of the thickness of the water film and

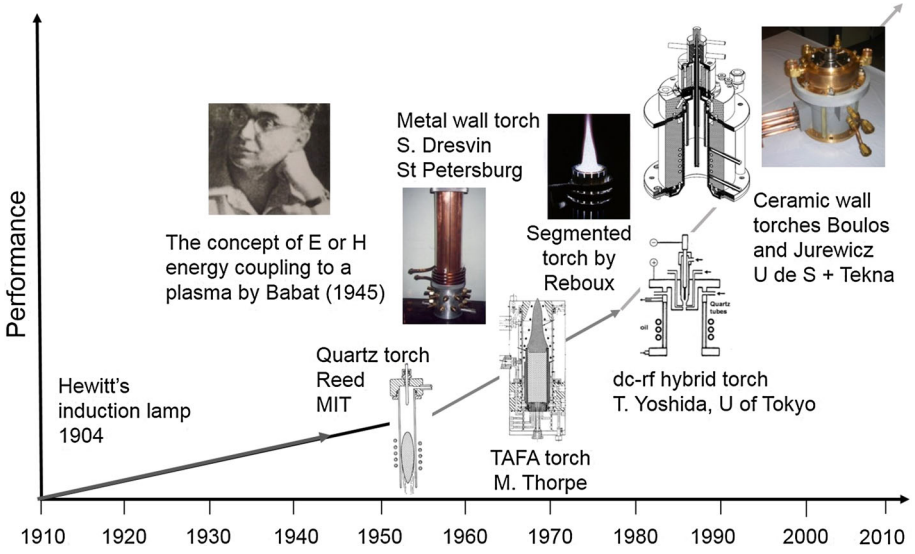

Fig. 2 Mile-stones in induction plasma torch development

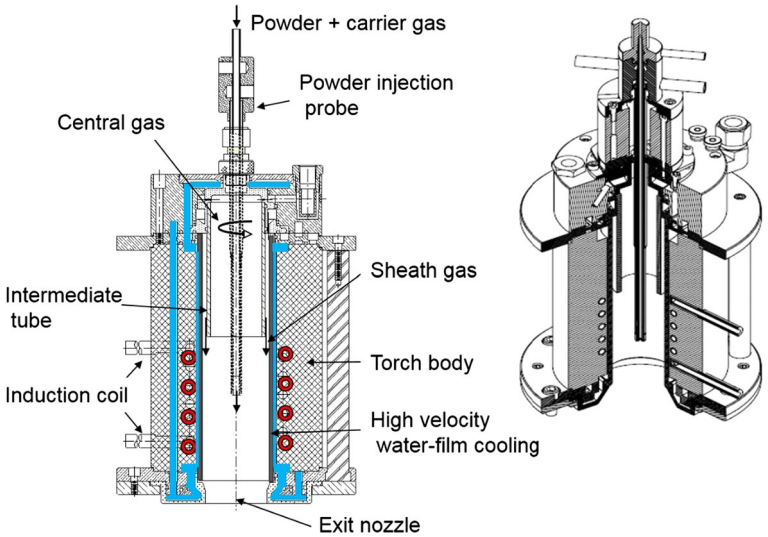

Fig. 3 Schematic representation of the basic design of the Tekna ceramic tube induction plasma torch. (Patents US 5200595, CAD 2085133, EP 533 884, JP 3169962, KR 203994, CN 92103380.X)

accordingly the velocity of the cooling-water flow over the outer surface of the ceramic tube.

- Precise control of the gas flow pattern in the discharge cavity.
- Incorporation of a water-cooled discharge nozzle, and a front mounting flange, which allows for precise control of the plasma jet at the exit of the torch and for operation of the torch in the subsonic and supersonic flow regimes.

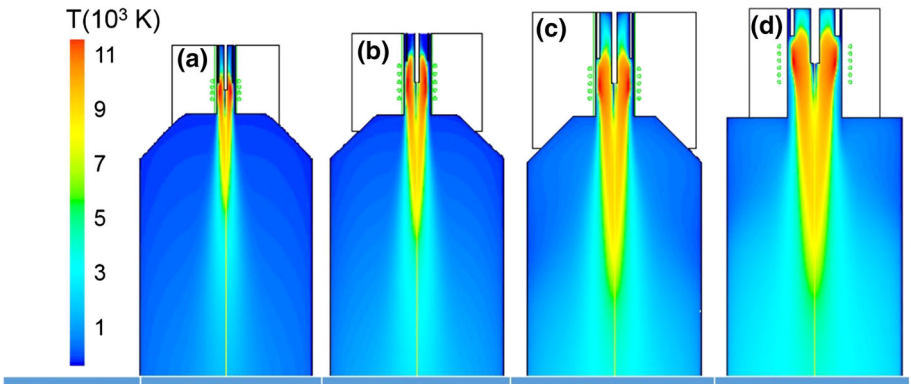

Torch	PS-35	PS-50	PS-70	PS-100
Power (kW)	40	60	100	200
Powder (slm)	5 Ar	5 Ar	5 Ar	5 Ar
Central (slm)	15 Ar	30 Ar	30 Ar	60 Ar
Sheath (slm)	80Ar+10H_2	100Ar+20H_2	120Ar+15H_2	250Ar+50H_2

Fig. 4 Temperature fields for different induction plasma torches, models PS-35 through PS-100, operating with Ar/H_2 as the plasma gas, at atmospheric pressures and different plate power ratings

Transport phenomena and plasma modelling has played a key role in the further development of this basic design of plasma source and its scaling-up to the hundred kW's power level [60–74]. Significant developments in this areas were also reported by Colombo and his collaborators at the University of Bologna [75–82]. These mostly dealt with three-dimensional modelling of the flow, temperature and concentration fields in the induction plasma under a wide range of conditions including single and multiple induction coil configurations.

Figure 4 shows typical temperature fields in the discharge for different induction plasma torch sizes, ranging from the PS-35 to the PS-100. The number associated with the torch model is an indication of the dimension in (mm) of the internal diameter of the plasma confinement tube. These torches were operated with a sheath gas (Q_3), composed of a mixture of Ar/H_2, the central gas (Q_2) and the powder carrier gas (Q_1) were of pure Ar. The computations were carried out for plate powers varying between 40 and 200 kW, at atmospheric pressure. In all of these cases, the energy coupled into the discharge was based on experimental measurements, which was generally around 65 % of the plate power. The corresponding radial profiles of the temperature of the plasma at the exit level of the torch are shown in Fig. 5. The axial profiles of the temperature and axial velocity of the plasma, along the centerline of the flow are shown in Fig. 6. It may be noted from Fig. 5 that with the increase of the diameter of the plasma confinement tube, and of the plasma power, the temperature distribution over most of the discharge region remains essentially uniform, with a maximum temperature of the discharge around 9500 to 10,000 K. However, as shown in Fig. 6, the length of the high temperature zone increases significantly with the increase of the discharge power. The maximum velocity at the exit of the torch remains essentially constant around 80 m/s. The velocity of the plasma is, however, directly affected by the ambient pressure of the discharge, increasing significantly when operating at reduced pressures.

Developments of the induction plasma source was also devoted to the scale-up of the technology to the hundreds of kW's power levels using high efficiency solid-state power supplies. These however had two principal technological limitation

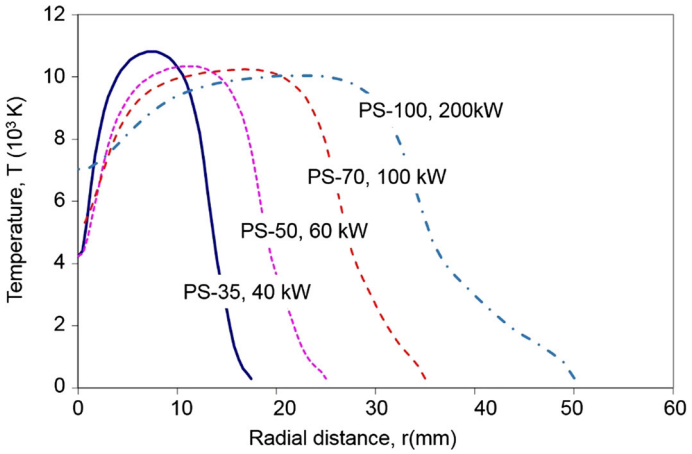

Fig. 5 Radial temperature profiles at the exit level of the torch for different plasma torches, models PS-35 through PS-100 operating with Ar/H_2 as the plasma gas, at atmospheric pressures and different plate power ratings

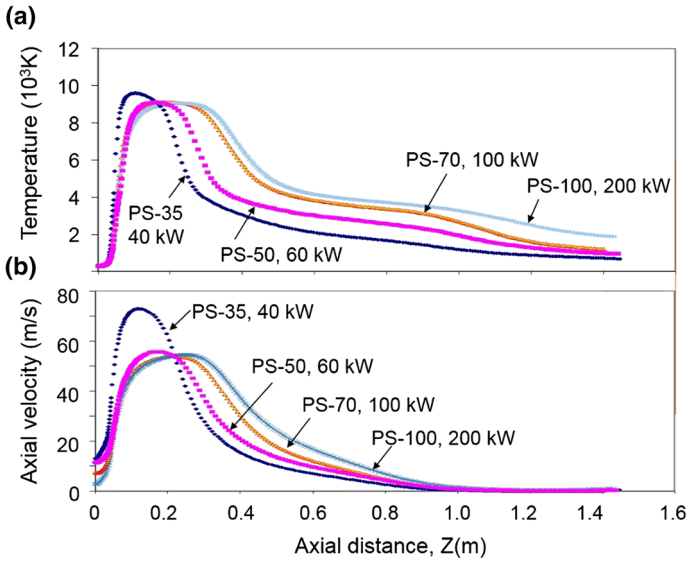

Fig. 6 Axial profiles of the temperature and axial velocity along the centerline for different plasma torches, models PS-35 through PS-100 operating with Ar/H_2 as the plasma gas, at atmospheric pressures and different plate power ratings

1. High-power solid-state power supplies that could be used for plasma generation are available for operation at frequencies in the 200–400 kHz range. Operation at high frequencies up to 1 MHz is possible at the cost of a drop of energy efficiency.
2. Most of the available solid-state power supplies operate at lower voltages and high coil currents, than corresponding vacuum tube oscillator units.

Faced with these constraints, two solutions were developed at Tekna Plasma Systems Inc. through extensive modeling and experimental work. The first is the multi-coil induction plasma torch shown in Fig. 7. This was developed essentially on the basis of Tekna's standard torch, illustrated in Fig. 3, with the exception of using four independent, coaxial, induction coils. The first of which on the upstream end of the torch is connected to a high frequency ($\sim$MHz), vacuum-tube rf power supply, while the remaining three (3) coils are connected in parallel, to a lower-frequency ($\sim$180 kHz), solid-state power supply. Torch ignition was initiated at low pressure using the high frequency coil. Once ignition was achieved, the lower frequency power supply is switched on with a gradual increase of its power setting. Stable operation could be achieved for an Ar/O_2 plasma (85.5 vol% O_2) at reduced pressure (27.5 kPa). The plate power of the high frequency power supply was 51 kW, while the power supplied by the solid-state unit was 291 kW, for a total of 342 kW. The power coupled into the discharge was experimentally measured at 300 kW which represented a plate coupling efficiency close to 88 % which is significantly higher than corresponding plate coupling efficiencies of (65 %) normally obtained with regular vacuum tube oscillator power supplies.

Subsequent work in this area, on the torch and power supply designs, led to the development of the PE-100 torch series which could be ignited and operate with a single solid-state power supply developed specifically for this application by EFD-Induction in Norway. The oscillator frequency was 280 kHz, the plasma gas was a mixture of Ar/N_2

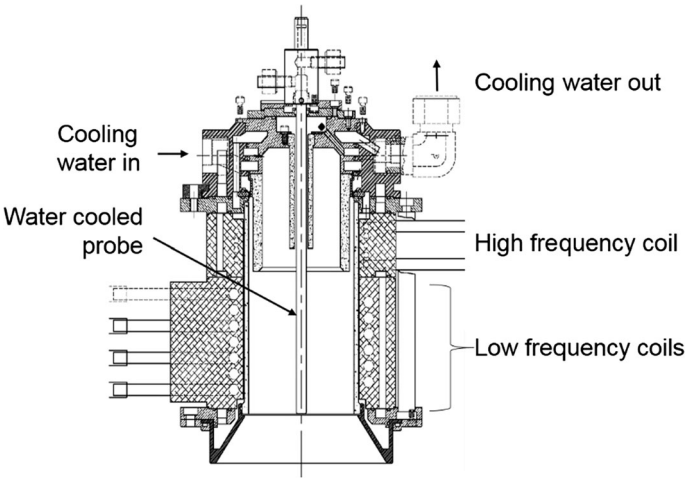

Fig. 7 Schematic representation of Tekna's multi-coil induction plasma torch. (Patents US 6693253, US 6919527, CAD 2462067, EP 1433366, JP 4317451, KR 890630, CN ZL02820827.7, RU 2295206)

(60 vol% N_2) with a total flow rate of 410 slm. Operation was tested at torch pressures of 46 and 56 kPa. Typical results are given in Fig. 8, Showing the power distribution in the torch, and the energy coupling efficiency (η_c) as function of the applied power. The energy coupling efficiency was defined in this case as the ratio of the energy coupled into the discharge to the DC power of the generator. It was generally around 75 %. Energy losses to the cooling circuit of the torch and the central injection probe was around 32 % of the power coupled into the discharge. The balance represents the energy in the plasma jet at the exit of the troch which is recovered in the cooling circuit of the reactor.

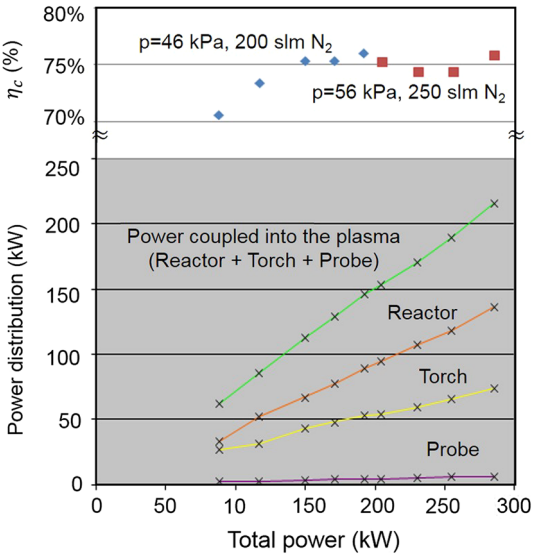

Fig. 8 Energy balance data for Tekna's PE-100 torch operating using a single solid-state power supply at a frequency of 280 kHz, Sheath gas = 100 slm (Ar) +200 or 250 slm (N_2), central gas = 50 slm (Ar), probe gas = 10 slm (Ar), pressure = 46 or 56 kPa

Induction Plasma Powder Treatment

The in-flight treatment of powders under plasma conditions has been one of the earliest and rapidly growing areas of induction plasma technology for the production of high purity, high added value powders [39, 40]. The process, schematically represented in Fig. 9, involves simply the axial injection of the powder into the center of the discharge using an appropriate carrier-gas. As the powder enters into the discharge cavity, the individual particles are heated by conduction and convection, Q_{cv}, while they lose energy to the surrounding wall through radiation, Q_r. As shown in Fig. 9, for complete melting of the particles, the energy received by the particles during their trajectory in the plasma, Q_{net} which is the integral of the net energy received, over their residence time in the plasma, should be superior than the energy required for the heating of the particles to their melting temperature, latent energy of fusion, and a certain degree of superheat, with a, surface area of the particle, c_p, specific heat of the particle, m, mass of the particle, h, heat transfer coefficient, H_m, latent heat of fusion of the particle, T_∞, plasma temperature, T_s, surface temperature of the particle, T_m, melting temperature of the particle, T_w, internal wall temperature of the reactor chamber, σ, Stefan–Boltzman constant, ε, surface emissivity of the particle, τ, residence time of the particle in the discharge.

Numerous studies were carried out on the impact of particle loading on the flow and temperature fields in the discharge, and their subsequent influence on the efficiency of the treatment of the powder. Proulx et al. [68, 69] at the University of Sherbrooke reported one of the first 2-D models on loading effects for powder treatment under plasma conditions. This was followed by some of the most elaborate 3-D models by Bernardi et al. [76] and Colombo et al. [81] at the University of Bologna.

The phenomena is best demonstrated by microscopic examination of the Molybdenum powder treated in an induction plasma at different powder feed rates. Results given in Fig. 10, are for a powder with a particle size distribution in the range of 40–200 μm, and a mean value of 130 μm, injected into a 100 kW, Ar/H_2 plasma at feed rates varying between 7 and 25 kg/h. These show a drop of percentage of the spherical particles in the treated powder, with the increase of the powder feed rate beyond 15 kg/h. A corresponding loss in tap density, and of the flowability of the treated powder is also observed. The latter is indicated by the Hall flow index, defined as the time in seconds that is necessary for the flow of a 50 g sample of the powder through a funnel of standard dimensions. It is

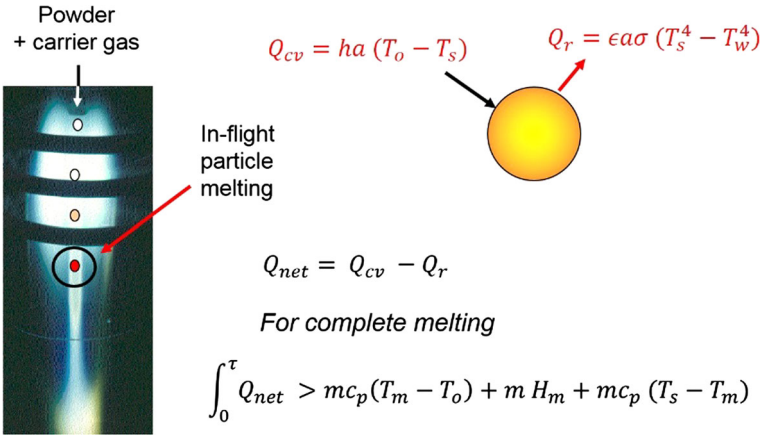

Fig. 9 Schematic representation of in-flight particle heating and melting in an induction plasma

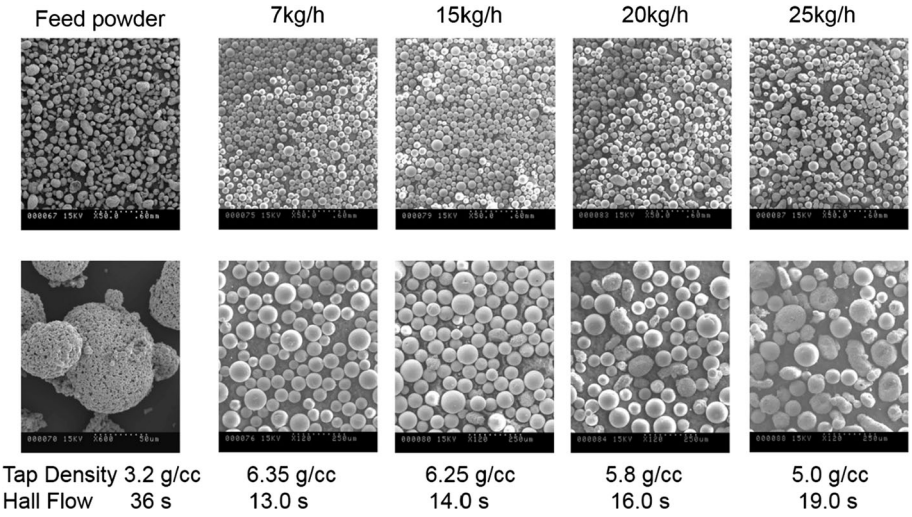

Fig. 10 Electron micrograph of Molybdenum powder treated into an atmospheric pressure, 100 kW, Ar/H_2 plasma, at different feed rates. **a** Feed material, 7.0, 15.0, 20.0 and 25.0 kg/h

observed from the data on Fig. 10 that the Hull flow value increases from 13 to 19 s/50 g with the increase of the powder feed rate from 7 to 25 kg/h.

The results of 2-D modelling work carried out on the same powder, with essentially the same plasma conditions are given in Fig. 11. These are summarized as follows:

Operational conditions for PS-70 torch
Plate power: 100 kW
Oscillator frequency: 3 MHz
Power to plasma 65 kW
Carrier gas flow rate: 8 slm Ar
Central gas flow rate: 40 slm Ar
Sheath gas flow rate: 125 slm Ar +25 slm H_2
Pressure: 110 kPa.
Mo particle feed rate: 7.5, 15 and 25 kg/h

The temperature fields in the discharge are given on the upper part of the figure, with the corresponding particle trajectories and their temperatures history for different Mo powder feed rates on the lower part of the figure. It may be noted that with the increase of the powder feed rate, the central region of the plasma jet becomes increasingly colder. The same effect is also observed on the temperature of the particle stream. In each of these cases, however, the particles moving along with respect to the particle stream reach a high temperature compared to those following a trajectory along the axis of the jet. The loading effect is also demonstrated by a gradual reduction of the compute mass fraction of the particles which are completely melted which drops from 100 % for feed rates up to 15 kg/h, to 67 % at a feed rate of 25 kg/h. The loading effect is also noted in Fig. 12, showing the local cooling of the central region of the plasma, as indicated by the radial profile of the plasma temperature at the exit level of the torch.

A schematic representation of the grid system used for the modelling of the system is given in Fig. 13. On the left hand side of the figure the particle size distribution of the Mo powder is represented by (n_ℓ) fractions with corresponding diameters, $d_p\,(\ell)$ and

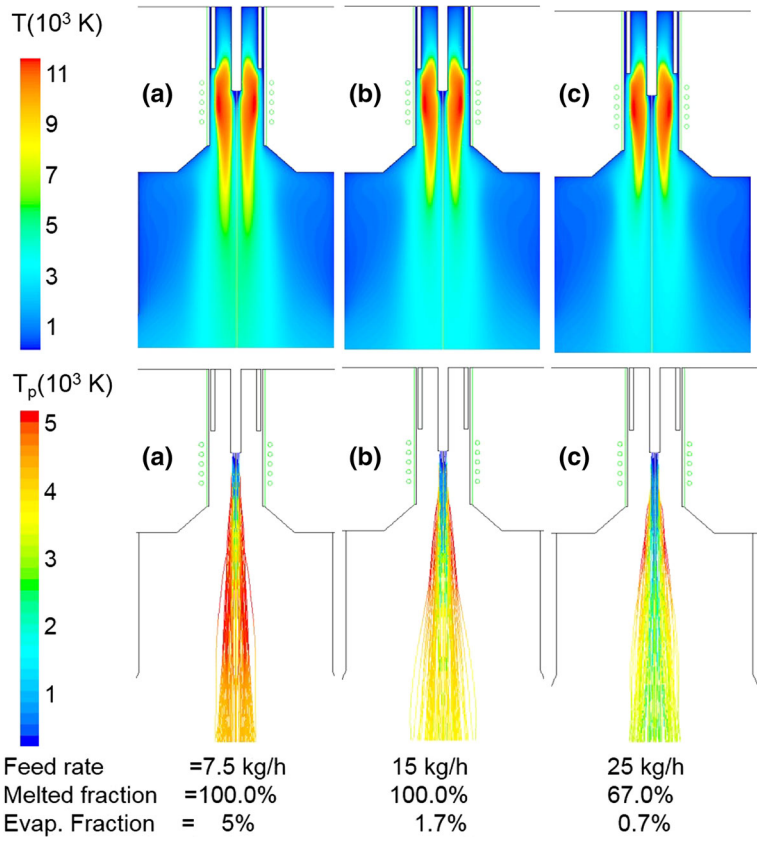

Fig. 11 Effect of the Mo powder feed rate on (*top*) the temperature fields in the discharge and (*bottom*) article trajectories and temperature as indicated by the *color code*, for a PN-70 torch mounted on a reactor of 250 mm i.d., Ar/H_2 plasma, 100 kW, 110 kPa

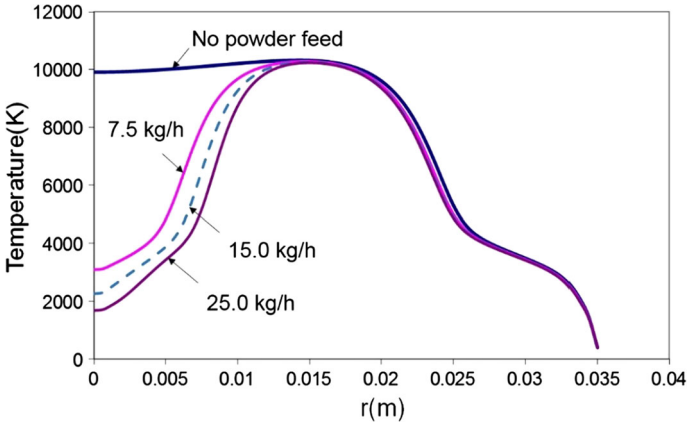

Fig. 12 Effect of Mo particle feed rate on the radial profiles of the plasma temperature at the exit level of the torch. Ar/H_2 plasma, 100 kW, 110 kPa

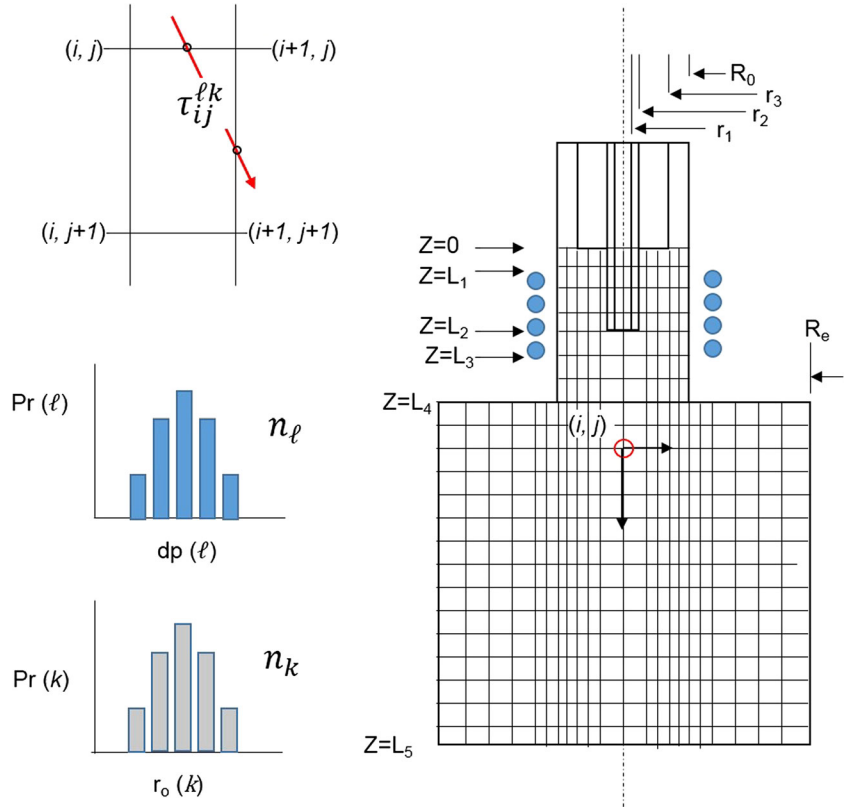

Fig. 13 Two-dimensional schematic representation of the grid structure used for the particle-source-in-cell model, the particle-size distribution of the feed powder and, their injection location into the flow

probabilities of, Pr (ℓ). Their corresponding injection location into the flow at the tip of the powder injection probe is represented by (n_k) locations at radial positions $r_o\,(k)$ and probabilities Pr (k). For a powder feed rate of m_p, the total number of particle trajectories to be computed is $(n_\ell \times n_k)$, with a corresponding residence time of each particle fraction in cell (i,j) being $(\tau_{ij}^{\ell k})$. It is to be noted that by definition;

$$\sum_{\ell=1}^{\ell=n_\ell} \Pr(\ell) = 1.0 \tag{1}$$

$$\sum_{k=1}^{k=n_k} \Pr(k) = 1.0 \tag{2}$$

In order to evaluate the loading distribution of the powder particles in the flow and their respective properties, computations were carried out using the standard 2-D modelling approach [69]. The results, however, were used further to calculate the following specific loading parameters which sheds light on the plasma-particle system.

a. *Particle mass loading distribution* x_{ij} (kg/m^3)

$$x_{ij} = \sum_{k=1}^{k=n_k} \sum_{\ell=1}^{\ell=n_\ell} x_{ij}^{\ell k} \Big/ v_{ij} \tag{3}$$

where, $x_{ij}^{\ell k}$ particle mass loading of cell ij, due to trajectory ℓk,

$$x_{ij}^{\ell k} = m_{p,\ell k} \cdot \tau_{ij}^{\ell k} \tag{4}$$

$m_{p,\ell k}$ powder mass flow rate along trajectory ℓk,

$$m_{p,\ell k} = m_p \cdot \Pr(\ell) \cdot \Pr(k) \tag{5}$$

$\tau_{ij}^{\ell k}$ time spent for particles on the trajectory ℓk, *in cell ij*, (s)
v_{ij} volume of an individual cell ij, (m^3)

b. *Particle number loading distribution* n_{ij} (m^{-3})

$$n_{ij} = \sum_{k=1}^{k=n_k} \sum_{\ell=1}^{\ell=n_\ell} n_{ij}^{\ell k} \Big/ v_{ij} \tag{6}$$

where, $n_{ij}^{\ell k}$ particle number loading of cell ij, due to trajectory ℓk (−)

$$n_{ij}^{\ell k} = \frac{x_{ij}^{\ell k}}{m_\ell} \tag{7}$$

m_ℓ mass of a single particle of size $d_{p\ell}$, (kg)

$$m_\ell = \frac{\pi d_{p\ell}^3 \rho_p}{6} \tag{8}$$

ρ_p density of the solid particle (kg/m^3)

c. *Particle mean temperature distribution* T_{ij} (K)

$$T_{ij} = \sum_{k=1}^{k=n_k} \sum_{\ell=1}^{\ell=n_\ell} m_{ij}^{\ell k} T_{ij}^{\ell k} \Big/ \sum_{k=1}^{k=n_k} \sum_{\ell=1}^{\ell=n_\ell} m_{ij}^{\ell k} \tag{9}$$

where, $m_{ij}^{\ell k}$ mass of particles on the trajectory ℓk, *in cell ij* (K), $T_{ij}^{\ell k}$ temperature of particles on the trajectory ℓk, *in cell ij* (K)

d. *Particle mean velocity distribution* v_{ij} (m/s)

$$v_{ij} = \sum_{k=1}^{k=n_k} \sum_{\ell=1}^{\ell=n_\ell} m_{ij}^{\ell k} v_{ij}^{\ell k} \Big/ \sum_{k=1}^{k=n_k} \sum_{\ell=1}^{\ell=n_\ell} m_{ij}^{\ell k} \tag{10}$$

where, $m_{ij}^{\ell k}$ mass of particles on the trajectory $\ell k, incellij$ (m/s), $v_{ij}^{\ell k}$ velocity of particles on the trajectory ℓk, *in cell ij* (m/s)

e. *Solid-to-gas mass loading ratio distribution* X_{ij} (−)

$$X_{ij} = x_{ij} / \rho_{g,ij} \tag{11}$$

where, $\rho_{g,ij}$ local plasma density in cell ij

f. *Particle surface loading distribution* s_{ij} $(\mathrm{m}^2/\mathrm{m}^3)$

$$s_{ij} = \sum_{k=1}^{k=n_k} \sum_{\ell=1}^{\ell=n_\ell} s_{ij}^{\ell k} \Big/ v_{ij} \tag{12}$$

where, $s_{ij}^{\ell k}$ particle surface loading of cell ij, due to trajectory ℓk (m^2)

$$s_{ij}^{\ell k} = n_{ij}^{\ell k} \cdot s_\ell \tag{13}$$

s_ℓ surface area of a single particle of size d_ℓ (m^2)

g. *Particule radiation distribution* $q_{r,ij}$ $(\mathrm{W}/\mathrm{m}^3)$

$$q_{r,ij} = \sum_{k=1}^{k=n_k} \sum_{\ell=1}^{\ell=n_\ell} \varepsilon \, \sigma \, s_{ij}^{\ell k} \left(T_{ij}^{\ell k} \right)^4 \tag{14}$$

h. *Solid-to-gas radiation ratio distribution* γ_R $(-)$

$$\gamma_R = q_{r,ij} / q_{g,ij} \tag{15}$$

where, $q_{g,ij}$ volumetric radiation from the gas phase at cell ij $(\mathrm{W}/\mathrm{m}^3)$

Figures 14a, shows the particle mass loading, x_{ij} $(\mathrm{kg}/\mathrm{m}^3)$ along the centerline of the plasma for different Mo powder feed rates. The powder transport gas flow rate is set at 10 slm (Ar). The corresponding values in terms of particle number loading, n_{ij} $(\mathrm{particle}/\mathrm{m}^3)$ is shown in Fig. 14b. It is noted that mass loading of the particles at the exit of the powder injection probe can be as high as 50 kg/m^3, for a powder feed rate of 25 kg/h. As the powder is entrained and dispersed into the discharge, the loading density drops rapidly to almost half of that value at the exit level of the torch reaching values below 5 kg/m^3 at around 150 mm from the exit of the torch. Because of the small size of the particles ($d_{50} = 130$ μm) the number density of the powder n_{ij} in the flow is of the order of 1.3×10^{10} $(\mathrm{particles}/\mathrm{m}^3)$ at the exit of the powder injection probe dropping down to $0.2–0.4 \times 10^{10}$ $(\mathrm{particles}/\mathrm{m}^3)$ at the exit level of the torch. At such a high particle density level (0.2×10^{10}), the mean distance between the particles is estimated at 793 μm, which corresponds to 6.1 particle diameters.

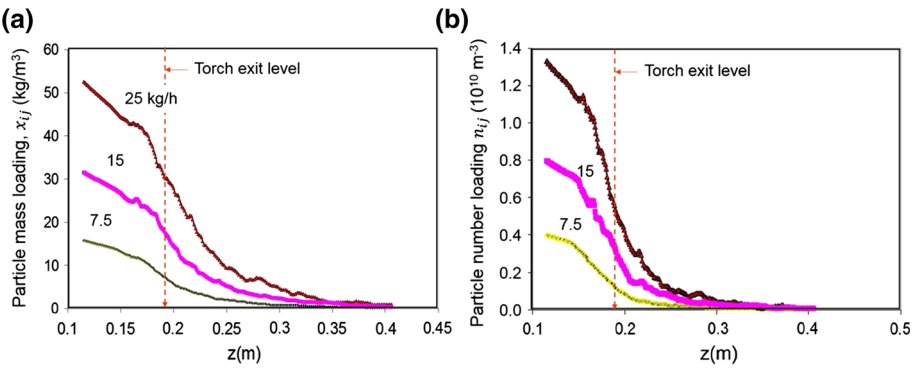

Fig. 14 Particle mass loading (**a**) and corresponding values of the particle number loading (**b**) along the centerline of the discharge, at different feed rates of Mo powder in a 100 kW Ar/H_2 plasma, 110 kPa

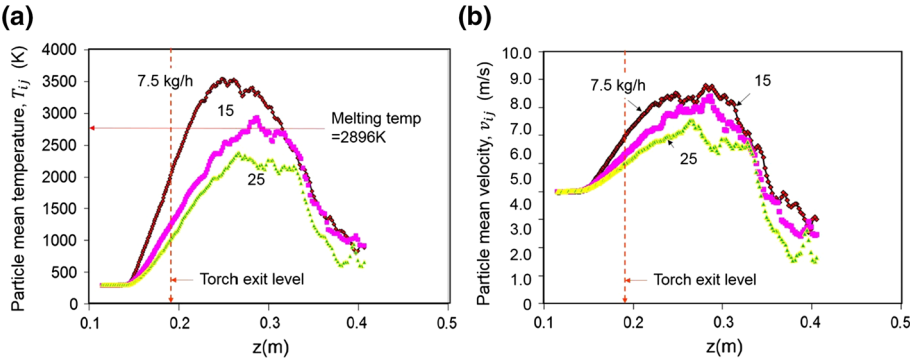

Fig. 15 Variation in the axial direction along the centerline of the discharge of **a** mean particle temperature, **b** mean axial velocity of the particles, at different feed rates of Mo powder in a 100 kW Ar/H_2 plasma, 110 kPa

The corresponding variation of the mean particle temperature and axial velocity along the centerline of the torch/reactor system are given in Fig. 15a. As indicated by Eqs. (9) and (10), these are mass mean weighed values. They show a rapid increase of the mean particle temperature as they are entrained by the plasma reaching a maximum value at about 50–100 mm from the exit level of the torch. As is expected, the maximum mean temperature of the particles varies with the powder feeding rate. At a feed rate of 7.5 kg/h, the mean particle temperature reaches 3500 K which is significantly higher than the melting temperature of Molybdenum (2896 K). It is not surprising to find that the powder is fully melted under this condition, and that 5 % of the weight of the powder feed into the torch is evaporated along this trajectory. With the increase of the powder feed rate, the maximum mean particle temperature drops to 3000 K, at 15 kg/h and to 2300 K at 25 kg/h. The powder is fully melted in this case at a feed rate of 15 kg/h, but only 67 wt% of the feed powder is melted at a feed rate of 25 kg/h. The corresponding fractions of the powder evaporated in these two cases are 1.7 % at 15 kg/h, and 0.7 % at 25 kg/h respectively. The mean particle velocities along their axial trajectory are given in Fig. 15b. These also go through a maximum in the range of 7–9 m/s, at about the same region of the flow where the particle temperature reaches its maximum value.

The corresponding particle surface density loading s_{ij} (m^2/m^3) along the axis of the jet can be calculated as shown by Eqs. (12) and 13). The results are given in Fig. 16a in terms of the axial profiles of the cumulative surface area of all the particles per unit volume of the plasma along the centerline of the plasma torch. Knowing the corresponding particle temperature, and accordingly its radiation intensity, it is possible to compute the total volumetric radiation intensity of the particle cloud $q_{r,ij}$ (W/m^3) as shown by Eq. (14). The results presented in Fig. 16b, show that the radiation form the solid particles, per unit volume of the plasma, can reach values as high as 30–50 $\times$ 10^6 W/m^3. Such volumetric radiation intensities are comparable to the volumetric radiation values for an atmospheric pressure argon plasma at around 8000 K. It should be underlined that heat loss from the surface of the particles injected into the plasma contributed to the thermal loading effect is in addition to the normal radiation emission from the plasma surrounding the particles.

Based on the above modelling results, it is possible to calculate the following integral parameters of the energy exchange between the plasma and the particles during the different parts of their trajectories in the flow;

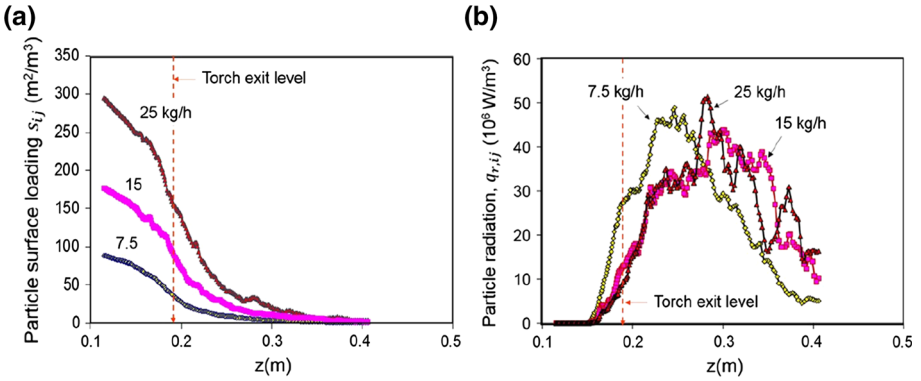

Fig. 16 Variation in the axial direction along the centerline of the discharge of **a** total particle surface area per unit volume, **b** total radiation density from the surface of the particles, at different feed rates of Mo powder in a 100 kW Ar/H_2 plasma, 110 kPa

$Q_{p,torch}$ power transferred from the plasma to the particles during their trajectory in the plasma torch cavity (kW)

$Q_{p,tot.}$ power transferred from the plasma to the particle during their complete trajectory (kW)

$Q_{p,rad.}$ radiation lost from the particle to the walls of the plasma torch and reactor chamber during their complete trajectory (kW)

The specific energy received by the particles (*SEP*) that contributes to the heating and melting of the particles can be calculated as,

$$SEP = \frac{Q_{p,tot} - Q_{p,rad.}}{m_p} \text{ (kWh/kg)} \tag{16}$$

where, m_p is the powder feed rate. The corresponding results for the three powder feed rates under consideration for the treatment of Mo powder in a 100 kW, Ar/H_2 plasma are summarized in Table 1.

It may be noted that the particles receive less than half of their total thermal energy during their trajectory in the plasma torch cavity. Moreover, throughout their full trajectory in the plasma flow, more than half of the energy received in-flight, is lost to the surrounding through radiation from the surface of the particles. That is to say that in order to achieve the complete melting, the particles will need to receive from the plasma, more than double of the Thermodynamic Specific Energy Requirement $(SER)_{TD}$ defined as;

$$(SER)_{TD} = c_{ps}(T_m - T_o) + H_m \text{ (kWh/kg)} \tag{17}$$

Table 1 Energy balance for the in-flight heating and melting of Mo particle at different powder feed rates, 100 kW, Ar/H_2 plasma, 110 kPa

m_p (kg/h)	$Q_{p,torch}$ (kW)	$Q_{p,tot.}$ (kW)	$Q_{p,rad.}$ (kW)	*SEP* (kWh/kg)	x_m (%)	x_v (%)
7.5	2.7	5.35	2.91	0.32	100	5.2
15.0	3.7	8.56	4.99	0.23	100	0.46
25.0	4.5	12.6	7.42	0.21	67	0.19

where, c_{ps} specific heat of the particle material in its solid state, T_m melting temperature of the particle material, T_o initial particle temperature, H_m latent heat of fusion of the particle material

Based on the thermophysical properties of Mo, the Thermodynamic $(SER)_{TD}$ is estimated as 0.89 MJ/kg, or 0.249 kWh/kg. Comparing this number with the values of *SEP* in Table 1, it is noted that at the feed rates of 7.5 and 15 kg/h the values of *SEP* are larger or close to $(SER)_{TD}$, while for the case for a feed rate of 25 kg/h the value of *SEP* is lower than $(SER)_{TD}$ which implies that the powder as a whole will not be receiving enough energy for complete melting, which is consistent with the value of 67 % of the molten fraction given by the model.

It should be underlined that such results reflect local loading effect of the plasma and are directly linked to the particle trajectories. Different results can be obtained by changing any of the parameters affecting particle trajectories, such as the location of the tip of the powder injection probe, or of the probe tip design. Results in support of this statement were obtained by imposing on the particle stream at the exit of the powder injection probe a 15° dispersion angle. Such a feature can be incorporated into the details of the design of the injection probe as shown by the two photographs on Fig. 17a, b. which were obtained on a cold-flow model used for the development of their internal designs. The probe (a) on the left hand side of the figure representing a standard probe, while (b), on the right hand side of the figure representing a 'dispersion probe' in which the powders are dispersed in the flow using an appropriate amount of radial or tangential dispersion gas. The results of particle trajectory computations are given in Fig. 17c–e, for three cases. The trajectories and temperature history of the particles injected using a standard probe, are given in Fig. 17c, for Mo powder feed rate of 25 kg/h giving rise to powder melting fraction of 67 %. The results given in Fig. 17d, e are for a 15° angle dispersion probe at 25 and 30 kg/h Mo powder feed rates respectively. In both of these cases, a 100 % powder melting was achieved due to the improved dispersion of the powder in the plasma flow. The improved

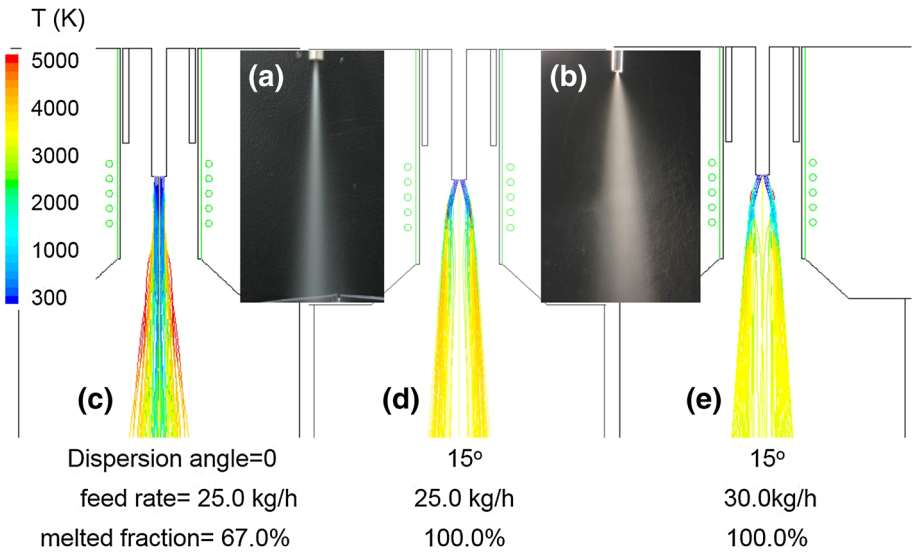

Fig. 17 Particle trajectories and temperature history using (**a**, **c**) standard powder injection probe and (**b**, **d**, **e**) 15° dispersion probe at different feed rates of Mo powder in a 100 kW Ar/H_2 plasma, 110 kPa. for a PN-70 torch mounted on a reactor of 250 mm i.d

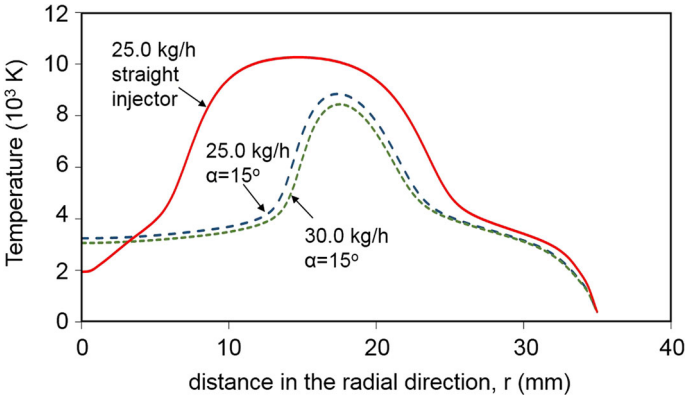

Fig. 18 Effect of dispersion angle on the radial temperature profiles of the plasma at the exit level of a PS-70 torch at different feed rates of Mo powder for an Ar/H_2 plasma at 100 kW, 110 kPa

distribution of the thermal load in this case is demonstrated in Fig. 18, giving the radial temperature profiles in the plasma at the exit level of the torch for these three cases.

In order to calculate the theoretical upper limit of the production capacity, $(m_p)_{max}$, of a given plasma system in a powder melting/spheroidization application it is necessary to evaluate both the power available for the process, P_n, and the specific energy required by the process, $(SER)_n$ as follows;

$$P_n = P_o - P_{wc} - P_{rad,v} - P_{resid} \tag{18}$$

$$P_{resid} = m_g \times h_{resid} \tag{19}$$

$$(SER)_n = (SER)_{TD} + (SRAD) \tag{20}$$

$$(m_p)_{max} = P_n / (SER)_n \tag{21}$$

where, P_o is the power coupled into the discharge $= \eta_o \times P_t$ (kW), η_o energy coupling efficiency, P_t plate power (kW), P_{wc} total wall losses by conduction and convention to the plasma torch (kW), $P_{rad,v}$ radiation losses from the plasma including additional radiation due to metallic vapors from the material being processed.(kW), P_{resid} residual power in the plasma that is at a temperature below the melting point of the material to be processed (kW), m_g mass flow rate of plasma gas (kg/h), h_{resid} specific enthalpy of the plasma gas at the melting temperature of the material being processed. (kWh/kg), $(SER)_{TD}$ thermodynamic specific energy requirement for the complete melting of the material (see Eq. (17) (kWh/kg), *SRAD* radiation losses from the particles during their trajectory until they are fully molten (kWh/kg).

For the case under consideration for the melting and spheroidization of Mo powder using a 100 kW (Ar/H_2) induction plasma source, with a coupling efficiency of 65 %, and a total gas flow rate of 200 slm (Ar/H_2) with an equivalent mass feed rate of plasma gas (18 kg/h).

$P_o = 65$ *kW,*
$P_{wc} = 1.2$ *kW (based on modelling results),*
$P_{rad,v} = 20$ *kW (based on modelling results)*

$P_{resid} = 18 \times 0.547 = 9.84\ kW$
$(SER)_{TD} = 0.25\ kWh/kg$
$SRAD = 0.65\ kWh/kg\ (based\ on\ modelling\ results)$

The theoretical Molybdenum powder melting capacity, $(m_{ps})_{max}$ is given by;

$$(m_{ps})_{max} = \frac{(65 - 1.2 - 20 - 9.84)}{(0.25 + 0.65)} = \frac{33.9}{0.9} = 37.7\ \text{kg/h}$$

Induction Plasma Synthesis of Nano-Powders

The plasma synthesis of nano-powders is another example of application of induction plasma technology for the preparation of specialized high quality ultrafine powders for a wide range of applications. The principal steps of the process are illustrated in Fig. 19. This involves essentially feeding the precursor in the form of fine solid powder, a liquid or a suspension. As the individual particles enter into contact with the plasma they are heated, melted and vaporized, forming a vapor cloud that mixes with the plasma flow. As the plasma gas, charged with the vapor of the precursor material, immerges from the vaporization section of the reactor, it is subjected to rapid cooling in the quench section either though contact with a solid surface, or through mixing with a cold quench gas stream. This sudden cooling of the plasma gas with its vapor charge results in the super-saturation of the plasma gas, and the condensation of the precursor material by homogeneous nucleation and growth. This leads to the formation or fine molten droplets that grows in size through the further condensation of the vapor on its surface or coagulation between adjacent droplets, until their final solidification in the form of ultrafine dispersed powder. The final particle size distribution of the condensed powder depends largely on the thermophysical properties of the material, the initial concentration of the vapor in the plasma stream, and the overall cooling rate to which the plasma with its vapor load are exposed during the quench step of the process.

Here again, the process development has been the subject of intense R&D efforts over the past four decades though a wide scope of experimental, and mathematical modelling studies which required a fundamental understanding of basic transport phenomena under these conditions. Typical results obtained for the vaporization of copper powder in a Tekna's PN-50, induction plasma torch mounted on a 200 mm i.d. reactor are given in

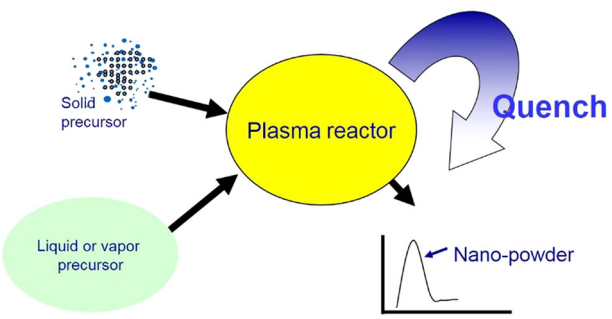

Fig. 19 Schematic representation of the synthesis of nano-powders through inflight heating, melting and vaporization of the precursor material followed by the rapid quench of the formed vapors leading to the condensation of the precursor in the form of an ultrafine powder

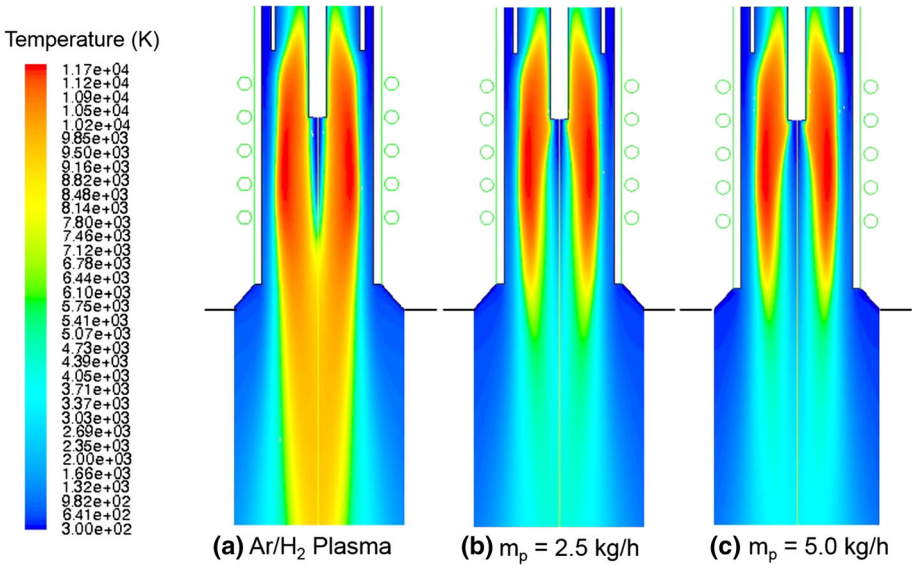

Fig. 20 Effect of copper powder vaporization on the temperature fields in the immediate vicinity of the plasma jet for a Tekna PN-50, Ar/H_2 (10.7 vol% H_2), at 60 kW and atmospheric pressure for powder feed rates of 2.5 and 5.0 kg/h. Powder dispersion angle $\alpha = 15°$. Plasma torch i.d. = 50 mm

Figs. 20 and 21. Figure 20 shows the temperature field in the plasma torch and the upper part of the reactor in an immediate vicinity of the plasma jet for an atmospheric pressure Ar/H_2 plasma with an average hydrogen concentration of 10.7 vol%, and a plate power of 60 kW. Based on experimental data, the energy coupling efficiency was estimated at 65 % which implies that 39 kW of the plate power was coupled into the discharge in the plasma torch. The results given in Fig. 20a, obtained in absence of any powder injection, show the conventional form of the discharge with a relatively small locally cooled region at the tip of the powder injection probe which reflects the local cooling of the plasma by the powder carrier gas which was maintained in his case at 10 slm (Ar) in the absence of any powder injection. Figure 20b, c shows the corresponding temperature fields in the presence of copper powder injection, with a particle size in the range of 30–60 μm, at a feed rates of 2.5 and 5.0 kg/h, respectively, with the same level of powder carrier gas. A significant local cooling of the plasma in the central region of the discharge is observed in both cases.

The corresponding particle trajectories and temperature history is shown in Fig. 21. These show a rapid heating of the copper particle in the early stages of their trajectory to temperature well above the melting point of copper (1356 K) reaching up to the its vaporization temperature (2868 K). Figure 21a, b also show the distribution of the mass fraction of the copper vapor into the discharge (x_{cu}) for copper powder feed rates of 2.5 and 5.0 kg/h respectively. It is interesting to note that, while the total amount of copper evaporated increases from 1.2 to 1.6 kg/h with the increase of the feed rate, the fraction of the feed powder evaporated, decreases from 44 to 32 wt% due to thermal loading effects. The effect is accompanied by the increase in copper vapor concentration in the plasma jet, at 5 kg/h compared to that at 2.5 kg/h.

The total radiation due to the copper vapor in the plasma, $Q_{r,Cu\ total}$, was computed for these two cases to be in the range of 21–22 kW which represents a significant thermal

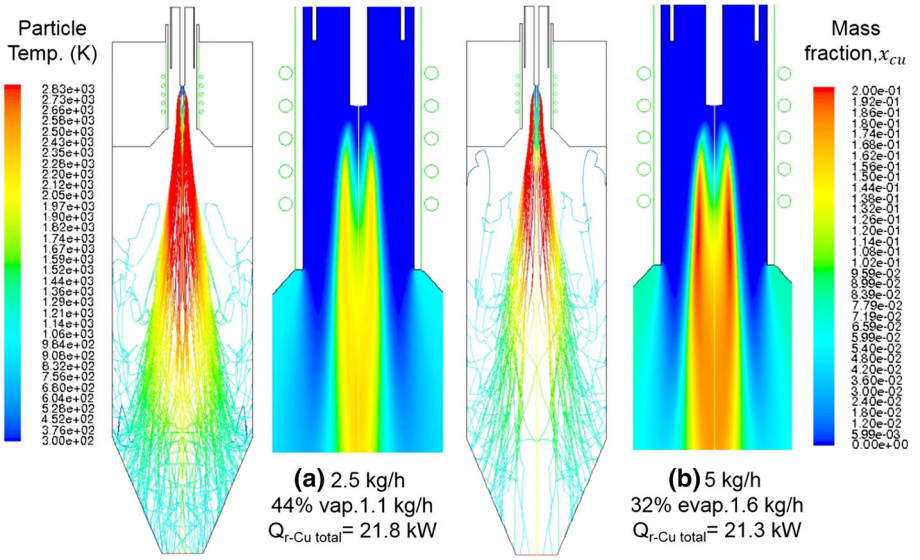

Fig. 21 Copper particle trajectories, particle temperature and mass fraction of copper vapor in the plasma, for **a** Tekna PN-50, mounted on a 200 mm i.d. reactor, Ar/H_2 (10.7 vol% H_2), at 60 kW and atmospheric pressure, for powder feed rates of 2.5 and 5.0 kg/h. Powder dispersion angle $\alpha = 15°$

loading of the plasma due to the presence of the copper vapors. This is in addition to the thermal loading caused by the copper particles inflight. The same equations presented above for the energy balance analysis for the case of powder spheroidization (Eqs. 18–21) also apply in the present case, with the exception that the $(SER)_{TD}$ should include two added terms for the heating of the molten particles to their vaporization temperature and for the latent heat of vaporization as follows.

$$(SER)_{TD} = m_p \cdot c_p s\,(T_m - T_o) + H_m + m_p \cdot c_{pl}(T_v - T_m) + H_v \tag{22}$$

For the case under consideration for the melting and vaporization of copper powder using a 100 kW (Ar/H_2) induction plasma source, with a coupling efficiency of 65 %, and a total gas flow rate of 200 slm (Ar/H_2), with an equivalent mass feed rate of (18 kg/h).

$P_o = 65$ *kW,*
$P_{wc} = 1.2$ *kW (based on modelling results),*
$P_{rad,v} = 25$ *kW (based on modelling results)*
$P_{resid} = 18 \times 1.753 = 31.6$ *kW*
$(SER)_{TD} = 1.639$ *kWh/kg*
SRAD = 0.15 kWh/kg (based on modelling results)

The theoretical copper powder evaporation capacity, $(m_{pv})_{max}$ is given by;

$$(m_{pv})_{max} = \frac{(65 - 1.2 - 25 - 31.5)}{(1.64 + 0.15)} = \frac{7.3}{1.79} = 4.1 \text{ kg/h}$$

Which is lower by almost one order of magnitude compared to possible powder processing capacity for same plasma power rating for a powder spheroidization process. The principal

parameters responsible for the significant decrease in the powder processing capacity for particle evaporation is the increase of the residual energy in the gases at temperature below the material vaporization temperature, and the increase of the plasma radiation losses due to the presence of the copper vapors.

Summary and Conclusions

A review is presented of principal technological developments in the field of thermal plasmas over the past half a century. This is followed by a discussion of the role played by transport phenomena and modeling for technology development. Examples are given for plasma source development where mathematical modeling was instrumental for the dimensioning of the plasma torch design and for evaluating the flow and temperature field under different operating conditions. The role of modeling is further discussed for process development for the cases of powder melting and spheroidization, and nano-powder synthesis through powder vaporization and condensation under plasma conditions. For these two cases calculation procedures are proposed for the estimation of potential powder processing capacity as function of the plasma power and the thermophysical properties of the material being processed. The results can be used as a guide for process optimization and potential improvements of process efficiencies.

Acknowledgments I would like to thank in particular the many graduate students, post-doctoral research fellows, research associates and colleagues who contributed through my career to this research program at the University of Sherbrooke. The financial supported by the National Sciences and Engineering Research Council of Canada and the Ministry of Education of the Province of Quebec are gratefully acknowledged. The reported mathematical modelling work was carried out by Dr Siwen Xue, and the experimental results were obtained by the research team, on the pilot R&D facility at Tekna plasma Systems Inc. whose contributions is gratefully acknowledged. Many thanks are due to Professor Jurewicz, for his time in reviewing this manuscript.

References

1. Stokes CS (1969) Chemistry in high temperature plasma jets. Adv Chem Ser 80:390–405
2. Vurzel FB, Polak LS (1970) Plasma chemical technology—the future of the chemical industry. Ind Eng Chem 62:8–22
3. Rykalin NN (1976) Plasma engineering in metallurgy and inorganic materials technology. Pure Appl Sci 48:179–194
4. Barcza NA (1986) The development of large scale thermal plasma systems. J South Afr Inst Min Metall 86(8):317–333
5. Barza NA, Curr TR, Jones TR (1990) Metallurgy of the open-bath plasma processes. Pure Appl Chem 62(9):1761–1772
6. Feinman J (1987) Plasma technology in metallurgical processing. Iron and Steel Society, Warrendale
7. MacRae DR, Cowx M (1988) Plasma furnace treatments of electric arc furnace dust as demonstrated by Bethlehem-Tetronics. In: EPRI-CMP 88-2 report
8. Neuschutz D (1992) Plasma applications in process metallurgy. High Temp Chem Process 1:511–525
9. Jones RT, Curr TR (2006) Pyrometallurgy at Mintek. South African Institute of Mining and Metallurgy, Johannesburg
10. Mishra S (2012) Thermal plasma application in metallurgy plasma processing of materials. Lambert Academic Publishing, Germany, p 148
11. Moore C, Heanly CP, Cowx P (1989) Plasma tundish heating as an integral part of continuous casting. Steel Times Int 13(2):44–46
12. Neuschütz D (1996) Arc heating in the tundish with a graphite electrode in comparison to metallic plasma torch. In: Steel research no. 11

13. Neuschütz D (2000) Metallurgical applications of high power arc heating systems. High Temp Chem Process 4:309–321
14. Esser B, Gulhan A (1998) Flow field characterization of DLR's arc heated facilities L2K and L3K. In: Proceeding of the 3rd European symposium. On aerothermodynamics for space vehicles, November 24–26 (1998), ESTEC, Noordwijk, The Netherlands, ESA SP-426, Dec
15. Auweter-Kurz M, Wegmann T (1999) Overview of IRS plasma wind tunnel facilities. In: TRO educational note 8, Measurement techniques for high enthalpy and plasma flows, course held at the Von Karman Institute for fluid dynamics, Belgium October 25–29
16. Bletzinger P, Ganguly BN, Van Wei D, Garscadden A (2005) Plasmas in high speed aerodynamics, a topical review. J Phys D Appl Phys 38:R33–R57
17. Lenzner S, Auweter-Kurtz M, Heiermann J, Sleziona PC (1998) Energy distribution in an inductively heated plasma wind tunnel for re-entry simulation. In: AIAA-98-2937, 7th AIAA#ASME joint thermosphysics and heat transfer conference Albuquerque, NM, June 15–18, 1998
18. Nemchinsky VA, Severance WS (2006) What we know and what we do not know about plasma cutting. J Phys D Appl Phys 39:R423–R438
19. Finch R (2007) Welder's handbook, a guide to plasma cutting, oxyacetylene, ARC, MIG and TIG welding. Revised HP1513
20. Colombo V, Concetti A, Ghedini E, Dallavalle S, Vancini M (2009) High-speed imaging in plasma arc cutting: a review and new developments. Plasma Sour Sci Technol 18:023001
21. Hirata Y (2011) Plasma physics promotes progress of arc welding processes. In: 3rd international round table on thermal plasmas 31st Oct.–Nov. 4th. Glenburn Lodge, Johannesburg
22. Davies AC (2003) The science and practice of welding. Cambridge University Press, Cambridge. ISBN 0-521-43566-8
23. American Welding Society (2004) Welding handbook, welding processes, part 1. American Welding Society, Miami. ISBN 0-87171-729-8
24. Wilden J, Bergmann JP, Frank H (2006) Plasma transferred arc welding—modeling and experimental optimization. J Therm Spray Technol 15(4):779–784
25. Murphy AB, Tanaka M, Tashiro S, Sato T, Lowke JJ (2009) A computational investigation of the effectiveness of different shielding gas mixtures for arc welding. J Phys D Appl Phys 42:115205
26. Murphy AB (2010) The effects of metal vapor in arc welding. J Phys D Appl Phys 43:434001
27. Murphy AB, Tanaka M, Yamamoto K, Tashiro S, Lowke JJ, Ostrikov K (2010) Modelling of arc welding: the importance of including the arc plasma in the computational domain. Vacuum 85:579–584
28. Murphy AB (2011a) Understanding the arc plasma in arc welding: recent progress and outstanding issues. In: 3rd round table on thermal 31st. Oct.–4th. Nov. Glenburn Lodge, Johannesburg
29. Murphy AB (2011b) A self-consistent three-dimensional model of the arc, electrode and weld pool in gas–metal arc welding. J Phys D Appl Phys 44:194009
30. Fauchais P, Heberlein JVR, Boulos M (2014) Thermal spray fundamentals, from powder to part. Springer, New York
31. Fauchais P, Vardelle A, Dussoubs B (2001) Quo vadis thermal spraying. J Thermal Spray Technol 10:44–66
32. Fauchais P (2004) Understanding plasma spraying. J Phys D Appl Phys 37:R86–R108
33. Fauchais P, Montavon G, Bernard G (2010) From powders to thermally sprayed coatings. J Thermal Spray Technol 19:56–80
34. Eschenbach RC (1989) Use of plasma torches for melting special metals and for destroying and stabilizing hazardous wastes. In: Proceedings of workshop industrial. Plasma Applications (Pugnochiuso)
35. Drouet MG (1992) High temperature processes for industrial waste treatment and valorization. In: Bonizzoni G et al (ed) Proceedings of international workshop on plasma technologies for hazardous waste destruction, Como, Italy. Editrice Compositori, Bologna, Italy, pp 77–88
36. Heberlein J (1992) Thermal plasmas for the destruction of hazardous wastes. In: Bonizzoni et al G (ed) Proceedings of plasma technologies for hazardous waste destruction, Como, Italy. Editrice Compositori, Bologna, pp 59–76
37. Murphy AB, McAllister T (2001) Modeling of the physics and chemistry of thermal plasma waste destruction. Phys Plasmas 8(5):2565–2571
38. Heberlein J, Murphy AB (2008) Thermal plasma waste treatment: a review. J Phys D Appl Phys 41:053001
39. Waldie B (1972) Review of recent work on the processing of powders in high temperature plasmas, part I processing and economic studies. Chem Eng 259:92
40. Waldie B (1972) Review of recent work on the processing of powders in high temperature plasmas, part II particle dynamics, heat transfer and mass transfer. Chem Eng 259:188

41. Boulos MI (1985) The inductively coupled R.F. (radio frequency) plasma. Pure Appl Chem 57:1321–1352
42. Ye R, Ishigaki T, Jurewicz J, Proulx P, Boulos' MI (2004) In-flight spherodization of alumina powders in Ar-H2 and Ar-N2 induction plasmas. Plasma Chem Plasma Process 24(4):555–571
43. Boulos MI (2002) Induction plasma synthesis and processing of nanostructured materials. In: IMP2002, Niyagi, Japan, November 27–29
44. Boulos MI (2012) New frontiers in thermal plasmas, from space to nano-materials. Nucl Eng Technol 44:1–7
45. Guo J, Xiaobao F, Dolbec R, Xue S, Jurewicz J, Boulos M (2010) Development of nanopowder synthesis using induction plasmas. Plasma Sci Technol 12(2):188
46. Mendoza Gonzalez NY, El Morsli M, Proulx P (2008) Production of nanoparticles in thermal plasmas: a model including evaporation, nucleation, condensation, and fractal aggregation. J Therm Spray Technol 17:533–550
47. Shigeta M, Murphy AB (2011) Thermal plasmas for nanofabrication. J Phys D Appl Phys 44:174025
48. Reed TB (1961) Induction coupled plasma torch. J Appl Phys 32:821–824
49. Dresvin SV (ed) (1971) Physics and technology of low temperature plasmas. Iowa State University, 1977
50. Thorpe ML, Scammon LW (1968) Induction plasma heating: high power, low frequency operation and pure hydrogen heating. In: NASA 3-9375, 1968
51. Yoshida T, Nakagawa K, Harada T, Akashi K (1981) New design of a radio frequency plasma torch. Plasma Chem Plasma Process 1:113–129
52. Yoshida T, Tawi T, Nishimura H, Akashi K (1983) Characterization of a hybrid plasma and its application to a chemical synthesis. J Appl Phys 54:640–646
53. Yoshida T, Tani T, Nishimura H, Akashi K (1983) Characterization of a hybrid plasma and its application to a chemical synthesis. J Appl Phys 54:640–646
54. Boulos MI (1976) Flow temperature field in the fire ball of an inductively coupled plasma. IEEE Trans Plasma Sci PS-4:28–39
55. Boulos MI (1978) Heating of powders in the fire ball of an induction plasma. IEEE Trans Plasma Sci PS-6:93–106
56. Boulos MI, Jurewicz J (1993) High performance induction plasma torch with a water-cooled ceramic confinement tube. US Patent, 5,200,595
57. Boulos MI, Jurewicz J (1996) Liquid film stabilized induction plasma torch. US Patent, 5,560,844
58. Boulos MI, Jurewicz J (2004) Multi-coil induction plasma torch for solid state power supply. US Patent 6,693,253, Feb 17th
59. Boulos MI, Jurewicz J (2005) Multi-coil induction plasma torch for solid state power supply. US patent 6,919,527 July 19th
60. Chen K, Boulos MI (1992) Turbulence in induction plasma modeling. J Phys D Appl Phys 27:946–952
61. El-Hage M, Mostaghimi J, Boulos MI (1989) A turbulent flow model for the R.F. inductively coupled plasma. J Appl Phys 65:4178–4185
62. Merkhouf A, Boulos MI (1998) Integrated model for the radio-frequency induction plasma torch and power supply. Plasma Sour Sci Technol 7:599–606
63. Merkhouf A, Boulos MI (2000) Distributed energy analysis for an integrated radio frequency induction plasma system. J Phys D Appl Phys 33:1581–1587
64. Mostaghimi J, Proulx P, Boulos MI (1984) Parametric study of the flow and temperature fields in inductively coupled plasma torch. Plasma Chem Plasma Process 4:199–217
65. Mostaghimi J, Proulx P, Boulos MI (1987) A two-temperature model of the inductively coupled R.F. plasma. J Appl Phys 61:1753–1760
66. Mostaghimi J, Boulos MI (1989) Two-dimensional electromagnetic field effects in inductively coupled plasmas. Plasma Chem Plasma Process 9:25–44
67. Mostaghimi J, Boulos MI (1990) Effect of frequency on local thermodynamic equilibrium conditions in an inductively coupled argon plasma at atmospheric pressure. J Phys D Appl Phys 68:2643–2648
68. Proulx P, Mostaghimi J, Boulos MI (1985) Plasma-particle interaction effects in induction plasma modelling under dense loading conditions. Int J Heat Mass Transf 28:1327–1336
69. Proulx P, Mostaghimi J, Boulos MI (1987) Heating of powders in an R.F. inductively coupled plasma under dense loading conditions. J Plasma Chem Plasma Process 7:29–53
70. Chen X, Merkhouf A, Boulos MI (1996) Preliminary study of the 3-equation turbulence model of an R.F. plasma torch. In: Proceedings of the 3rd Asia-Pacific conference on plasma science and technology, vol 1, Tokyo, pp 71–76
71. Selezneva S, Sember V, Gravelle DV, Boulos MI (2002) Spectroscopic validation of the supersonic plasma jet model. J Phys D Appl Phys 35:1338–1349

72. Xue S, Proulx P, Boulos MI (2001) Extended-field electromagnetic model for the inductively coupled plasma. J Phys D Appl Phys 34:1897–1906
73. Xue S, Proulx P, Boulos MI (2003) Effect of coil angle in an inductively couple plasma torch: a novel two-dimensional model. Plasma Chem Plasma Process 23:245–263
74. Ye R, Proulx P, Boulos MI (1999) Turbulence phenomena in the RF induction plasma torch. Int J Heat Mass Transf 42:1585–1595
75. Bernardi D, Colombo V, Ghedini E, Mentrelli A (2003) Three-dimensional modelling of inductively coupled plasma torches. Eur Phys J D 22:119–125
76. Bernardi D, Colombo V, Ghedini E, Mentrelli A, Trombetti T (2004) 3-D numerical simulation of fully-coupled particle heating in ICPTs. Eur Phys J D 28:423–433
77. Bernardi D, Colombo V, Ghedini E, Mentrelli A (2005) 3-D turbulent modelling of an ICPT with detailed gas injection section. IEEE Trans Plasma Sci 33:426–427
78. Bernardi D, Colombo V, Ghedini E, Mentrelli A (2005) Three-dimensional modelling of inductively coupled plasma torches. Pure Appl Chem 77:359–372
79. Colombo V, Ghedini E (2007) 3-D modeling of ICP torches. High Temp Mater Proc 11:283–296
80. Colombo V, Ghedini E, Sanibondi P (2010) A three-dimensional investigation of the effects of excitation frequency and sheath gas mixing in an atmospheric-pressure inductively coupled plasma system. J Phys D Appl Phys 43(105202):1–14
81. Colombo V, Ghedini E, Sanibondi P (2010) Three-dimensional investigation of particle treatment in a RF thermal plasma with reaction chamber. Plasma Sources Sci Technol 19(065024):1–13
82. Colombo V, Concetti A, Ghedini E, Gherardi M, Sanibondi P (2011) 3-D time-dependent large eddy simulation of turbulent flows in an inductively coupled thermal plasma torch with reaction chamber. IEEE Trans Plasma Sci 39:2894–2895